

## Elucidating the effect of cohesive zone length in fracture simulations of particulate composites

Ponnusami, Sathiskumar Anusuya; Krishnasamy, Jayaprakash; Turteltaub, Sergio; van der Zwaag, Sybrand

**DOI**

[10.1016/j.engfracmech.2022.108431](https://doi.org/10.1016/j.engfracmech.2022.108431)

**Publication date**

2022

**Document Version**

Final published version

**Published in**

Engineering Fracture Mechanics

**Citation (APA)**

Ponnusami, S. A., Krishnasamy, J., Turteltaub, S., & van der Zwaag, S. (2022). Elucidating the effect of cohesive zone length in fracture simulations of particulate composites. *Engineering Fracture Mechanics*, 268, Article 108431. <https://doi.org/10.1016/j.engfracmech.2022.108431>

**Important note**

To cite this publication, please use the final published version (if applicable). Please check the document version above.

**Copyright**

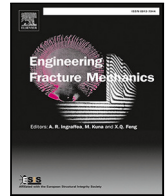
Other than for strictly personal use, it is not permitted to download, forward or distribute the text or part of it, without the consent of the author(s) and/or copyright holder(s), unless the work is under an open content license such as Creative Commons.

**Takedown policy**

Please contact us and provide details if you believe this document breaches copyrights. We will remove access to the work immediately and investigate your claim.

Contents lists available at [ScienceDirect](https://www.sciencedirect.com)

# Engineering Fracture Mechanics

journal homepage: [www.elsevier.com/locate/engfracmech](http://www.elsevier.com/locate/engfracmech)

## Elucidating the effect of cohesive zone length in fracture simulations of particulate composites

Sathiskumar Anusuya Ponnusami<sup>a</sup>, Jayaprakash Krishnasamy<sup>b</sup>, Sergio Turteltaub<sup>b,\*</sup>, Sybrand van der Zwaag<sup>b</sup>

<sup>a</sup> Department of Mechanical Engineering and Aeronautics, City, University of London, Northampton Square, London, EC1V 0HB, United Kingdom

<sup>b</sup> Department of Aerospace Structures and Materials, Faculty of Aerospace Engineering, Delft University of Technology, Kluyverweg 1, 2629 HS Delft, The Netherlands

### ARTICLE INFO

#### Keywords:

Fracture process zone  
Length scale  
Crack driving force  
Crack-particle interaction  
Cohesive zone fracture mechanics  
Particulate composites

### ABSTRACT

The influence of the cohesive zone length on the crack driving force is quantified and analyzed in a representative system of particles dispersed in a matrix of a composite material. For heterogeneous material systems, e.g. particulate composites, it is known that as a crack approaches the particles, the crack driving force may increase (shielding) or decrease (anti-shielding) depending on the relative stiffness of the particles. These results have been established in numerous studies using the classical linear elastic fracture mechanics approach (LEFM). The cohesive zone method (CZM) introduces a length scale parameter, referred to as the cohesive zone (or fracture process zone) length scale, into the formulation of fracture mechanics. It is generally established that fracture mechanics predictions using the CZM are similar to those obtained using LEFM in the limit case where the process zone is very small relative to a suitable characteristic dimension of the problem. However, the influence of the length scale parameter has not been clearly demonstrated for crack propagation in a heterogeneous material system, especially when the cohesive zone length is not negligible. By considering a simple crack-particle-matrix system, it is shown that, in addition to the elastic properties, the process zone length scale parameter exhibits a critical influence on the crack driving force. For this study, the concept of configurational forces is utilized and the eXtended Finite Element Method (XFEM) is employed as a tool to simulate crack propagation. Through numerical simulations, it is shown that (i) the magnitude of the driving force vector directly depends on the length scale parameter and (ii) the direction of the driving force is largely influenced by the presence of a cohesive zone. This, in turn, alters the crack trajectory in the particulate system if the criterion for the direction of crack propagation depends on the orientation of the driving force vector. Towards this end, two different criteria for direction of crack propagation, namely maximum principal stress and maximum energy dissipation, are compared in the presence of a cohesive zone and the results are reported. The study reveals the crucial influence of the inherent length scale associated with the cohesive zone method when applied to crack propagation in particulate composite systems and elucidates important differences when comparing predictions from distinct theories of fracture mechanics.

\* Corresponding author.

E-mail addresses: [Sathiskumar.Ponnusami@city.ac.uk](mailto:Sathiskumar.Ponnusami@city.ac.uk) (S.A. Ponnusami), [J.Krishnasamy-1@tudelft.nl](mailto:J.Krishnasamy-1@tudelft.nl) (J. Krishnasamy), [S.R.Turteltaub@tudelft.nl](mailto:S.R.Turteltaub@tudelft.nl) (S. Turteltaub), [S.vanderZwaag@tudelft.nl](mailto:S.vanderZwaag@tudelft.nl) (S. van der Zwaag).

<https://doi.org/10.1016/j.engfracmech.2022.108431>

Received 11 October 2021; Received in revised form 22 March 2022; Accepted 29 March 2022

Available online 12 April 2022

0013-7944/© 2022 The Author(s). Published by Elsevier Ltd. This is an open access article under the CC BY license (<http://creativecommons.org/licenses/by/4.0/>).

## 1. Introduction

Methods based on Linear Elastic Fracture Mechanics (LEFM) have been extensively used to study the change in the crack front driving force in the presence of particles in an otherwise homogeneous medium [1–11]. The key conclusion of those studies is that the crack driving force is amplified in the presence of a softer particle ahead of the crack tip and diminished if the particle is stiffer than the surrounding matrix material.

The aforementioned classical fracture mechanics approaches are based on a singular stress field at the crack front and a crack driving force that is characterized by a single scalar parameter such as the Stress Intensity Factor (SIF), the Strain Energy Release Rate (SERR) or the  $J$ -integral [12]. All these parameters directly or indirectly represent the amount of energy available at the crack front for crack propagation. The crack grows if the driving force parameter exceeds a critical limit, usually a material parameter such as fracture toughness or critical energy release rate.

From a different modeling perspective, another popular approach to analyze crack problems in particulate composites is the cohesive zone fracture mechanics, which introduces a process zone in front of the crack as opposed to the sharp crack front (or crack tip in plane stress or plane strain situations) [13–16]. In the cohesive zone formulation, the singular fields typical of LEFM are no longer present. Instead, the fracture process is described in terms of a constitutive relation in the form of a cohesive traction in the cohesive zone obtained as a function of the local crack opening. The conventional interpretation of the crack opening inside the cohesive zone is that of partially separated surfaces that can still transmit loads until the separation reaches a critical value beyond which the two crack surfaces are completely detached from each other. Cohesive zone modeling introduces an inherent length scale into the problem characterized by the *fracture process zone length*, which varies from small values for very brittle materials (with relatively low fracture energy and large fracture strength) to larger values for less brittle materials.

Studies exist in the literature on the comparison between cohesive zone and classical fracture mechanics approaches [17–22], some of which highlight the conditions under which the cohesive fracture mechanics coincides with classical fracture mechanics. One of the conclusions is that when the process zone is relatively small, the solutions obtained from cohesive fracture mechanics should coincide with that of the classical fracture mechanics. This is expected as the singular crack tip stress fields can be recovered when the process zone length tends to zero.

However, and relevant to the present work, less attention has been given in the literature to the *effect of the length scale parameter* in the context of *crack-particle interactions* in heterogeneous systems. Such a study on the effect of process zone length on fracture in particulate composite system deserves attention especially to reveal the toughening characteristics of particle reinforcement in materials with varying fracture process zone lengths. It is worth emphasizing that the strengthening or toughening in particle reinforced composites is principally governed by the crack shielding/antishielding and the resulting crack trajectory induced by the presence of the particles. Therefore, the objective of the present work is to quantify the effect of heterogeneous inclusions, such as reinforcing particles, on the crack propagation characteristics in the presence of a cohesive or process zone.

This analysis is carried out based on numerical simulations of representative cases of cracks propagating in a matrix in the vicinity of reinforcing particles. The crack propagation analysis using CZM does not provide *direct* quantification of the effect of particles on the crack driving force, as the approach does not involve parameters such as energy release rate or stress intensity factor to do so. Rather, the cohesive modeling framework invokes a constitutive relation in the cohesive zone which *implicitly* contains the crack driving force and the crack propagation kinetics. Consequently, in order to be able to interpret the results within a common framework, the concept of *configurational force*-based energy integrals is utilized as a tool to quantify the crack driving force in the presence of cohesive zone in a heterogeneous material.

The simulations are conducted using the eXtended Finite Element Method (XFEM) which enables the implementation of the cohesive zone approach through traction-separation relations. The XFEM also provides enhanced degrees of freedom to describe crack nucleation and propagation. The crack driving force is evaluated numerically using computationally-convenient expressions related to the configurational force of cracks. It is worth observing that if the cohesive zone model framework is used in an incremental quasi-static analysis, the configurational force itself is *not* required to determine the extent of crack growth, which can be established from an existing crack orientation, the condition of equilibrium and the constitutive information included in a traction-separation relation. Regarding the crack nucleation and the evolution of the crack orientation, these can also be modeled separately from the configurational force itself. Specifically, two distinct criteria, namely the maximum dissipation criterion and the maximum principal stress criterion, are used in the present work to determine the direction of crack propagation. Consequently, the evaluation of the configurational force is seen as a post-processing step to be able to quantify the effect of the process zone length on crack kinetics using the results of the numerical simulations.

The paper is organized as follows: The concept of configurational forces as applied to a crack in a heterogeneous material system is briefly discussed in Section 2, followed by a short description of the numerical implementation of cohesive zone modeling in XFEM in Section 3. The effect of process zone on the crack propagation kinetics in a particulate system is analyzed and the results are reported in Section 4 and Section 5. Firstly, the results of crack propagation analysis in particle-matrix system containing a pair of symmetrically located particles are reported in Section 4. This case is chosen to focus of the magnitude of the crack growth, which evolves on a straight path for all values of the cohesive zone length considered. Subsequently, the effect of process zone on crack path (direction of crack propagation) is discussed in Section 5 by involving a matrix crack interacting with a single particle located at an offset with respect to the initial crack direction. In this case, in addition to studying various cohesive zone lengths, two distinct criteria are also compared in terms of their crack path predictions. Summary and concluding remarks are provided in Section 6.

## 2. Configurational forces and thermodynamic driving forces for fracture problems in inhomogeneous systems

### 2.1. Background

Although the present work is carried out in the framework of the geometrically linear theory, the concept of configurational forces is better understood in the context of geometrically non-linear mechanics where the state of a (solid) material is described in a reference configuration. For purely elastic processes in a closed system, the reference configuration does not experience changes: the variables used to describe the geometry and the material behavior remain unchanged throughout a deformation process (only the values of the deformation and force fields evolve). However, whenever the material experiences an inelastic process such as fracture, phase transformation or plastic deformation, there are also changes in the reference configuration. In the case of fracture, the nucleation and growth of a crack alters the reference configuration as new surfaces are created and hence new material points need to be added to the kinematic description in the reference configuration representing the two new crack faces.

Configurational forces are interpreted as the energetically-conjugate quantities associated with material changes in the reference configuration [23]. A closely-related concept is the notion of the crack's thermodynamic driving force (i.e., a so-called *affinity*) as developed in the framework of classical irreversible thermodynamics. In fact, in the context of a simple material described without internal fracture variables and for an isolated crack described by a sharp crack front, the configurational force associated to the crack is equal to the negative of the crack's thermodynamic driving force [24].

One distinguishing factor of the theory of configurational forces is that balance principles are postulated for the configurational forces, which lead to field equations that need to be solved in addition to the (classical) balance principles of Newtonian mechanics. These field equations are augmented with constitutive information that connect the configurational forces to their conjugated quantities. These relations serve as the basis for crack propagation studies [25,26]. The theory of configurational forces has been applied to elasto-plastic fracture problems [27–29].

Simha et al. [24] extended the theory of configurational forces to account for the presence of smooth and discontinuous inhomogeneities in the material. The influence of inhomogeneities on the crack front driving force was quantified for the case of a two-phase material separated by a sharp interface in [30]. Several other studies utilize the configurational force approach to quantify the effect of interface (either a bimaterial planar interface or particle-matrix interface) [31–33].

In line with the approach developed in [24], the concept of configurational forces for a heterogeneous material system presented is adopted in this work, in which the inhomogeneities are particles separated from the matrix by sharp interfaces. In that case, the Helmholtz energy function and the stress and strain tensors are generally discontinuous across the particle/matrix interfaces. Regarding the crack front, two distinct modeling approaches can be considered, namely (i) a sharp crack front, related to the model given by Linear Elastic Fracture Mechanics and (ii) a diffuse crack front corresponding to the modeling approach connected to the Cohesive Zone Model. The expressions presented in [24] were developed for the case of a sharp crack front and these are formally extended here to include the case of a diffuse crack front, which essentially involves a re-interpretation of the contour integral on the crack front by the corresponding model. The system of equations based on configurational forces in the presence of particles is discussed below.

### 2.2. Configurational force for a crack

Consider a region  $\Omega$  that contains a crack front as shown in Fig. 1. The region  $\Omega$  also includes particles in the region  $\Omega_p$  embedded in the matrix that occupies the region  $\Omega_m$ . The external boundaries of  $\Omega$  consist of a so-called far-field boundary  $\Gamma_{\text{far}}$  (which is away from the crack front), the crack surfaces  $\Gamma_{\text{crack}}$  that are fully-separated, and a contour  $\Gamma_{\text{front}}$  which is asymptotically close to the crack front. The notion of 'far' and 'close' are interpreted in terms of the validity of the asymptotic fields associated to singular fields for sharp crack fronts. As illustrated in the inset of Fig. 1, the contour  $\Gamma_{\text{front}}$  is denoted as  $\Gamma_{\text{tip}}$  for the sharp crack front and referred to as  $\Gamma_{\text{coh}}$  for the diffuse crack front case. In addition to the external boundaries, and of special interest for the present work, the internal boundaries separating the particles and the matrix are collectively denoted as  $\Gamma_{\text{int}}$ . Adopting a similar convention as the one used in [24–26] for the orientation of the vectors, the outward normal unit vector to the far-field is denoted as  $\mathbf{n}$ , the inward unit vector to the crack front boundary is denoted as  $\mathbf{m}$  (inward with respect to  $\Omega$ ) while the normal to the internal boundaries is also denoted as  $\mathbf{m}$ , with the convention that it points outwards with respect to the particles  $\Omega_p$  (inward with respect to the matrix  $\Omega_m$ ).

#### 2.2.1. Configurational force for a sharp crack front

From thermodynamic considerations associated to the fracture process in the domain  $\Omega$  (namely the second postulate in the form of the Clausius-Duhem inequality for entropy production), it is possible to identify the thermodynamic driving force for a crack, denoted as  $\mathbf{J}_f$ , as the energetically-conjugated quantity to the crack front velocity, denoted as  $\mathbf{v}_f$ , such that the rate of energy dissipation  $D_f$  ascribed to the fracture process is non-negative for any possible process, i.e.,

$$D_f = \mathbf{J}_f \cdot \mathbf{v}_f \geq 0. \quad (1)$$

For the case of a sharp crack front (crack tip for plane problems) and assuming a geometrically linear framework in a plane strain or plain stress case, the crack driving force  $\mathbf{J}_f$  is equal to the negative of the configurational force  $\mathbf{f}_{\text{front}}$ , and is given by

$$\mathbf{J}_f = -\mathbf{f}_{\text{front}} = \int_{\Gamma_{\text{front}}} (\phi \mathbf{I} - \nabla \mathbf{u}^T \boldsymbol{\sigma}) \mathbf{m} ds \quad \Gamma_{\text{front}} \rightarrow \Gamma_{\text{tip}} \quad (2)$$

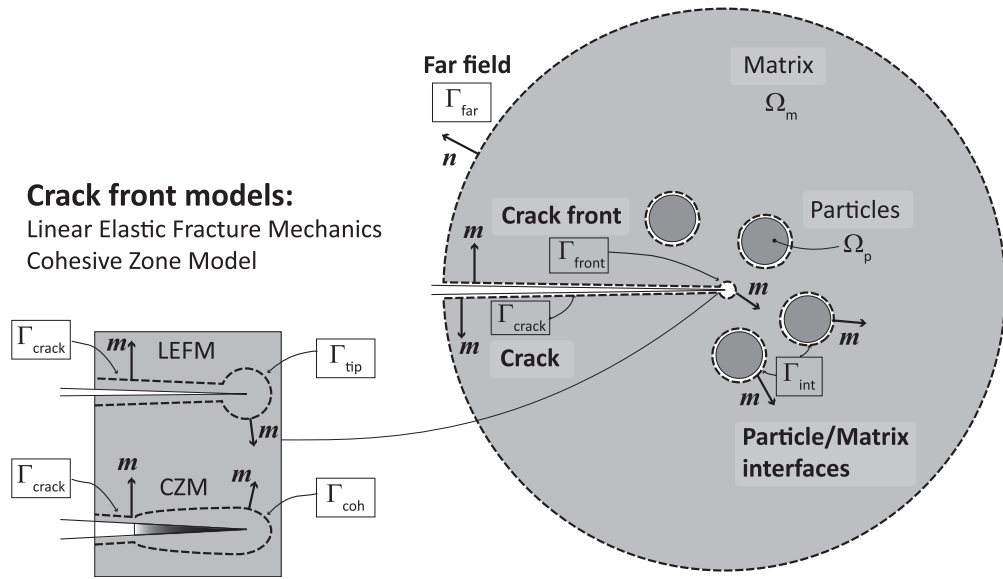


Fig. 1. Schematic of a neighborhood  $\Omega$  of a crack front in a heterogeneous material corresponding to a matrix occupying a region  $\Omega_m$  with embedded particles occupying a region  $\Omega_p$ . As shown in the inset, the crack front can be modeled as a sharp front, typically used in LEFM, or a diffuse, partially-damaged front, associated to the CZM. Observe the convention that  $n$  is an outward unit vector and  $m$  is an inward unit vector with respect to the matrix domain  $\Omega_m$ .

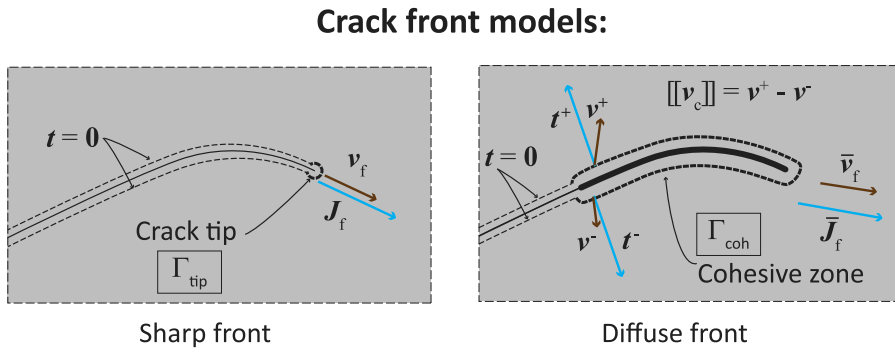


Fig. 2. Crack front models: Sharp front (left) typically used in an asymptotic analysis in Linear Elastic Fracture Mechanics and diffuse front (right) typically used in conjunction with Cohesive Zone Modeling.

with  $\phi$  being the Helmholtz energy density (which reduces to the strain energy density  $\phi_{\text{iso}} = \frac{1}{2} \sigma \cdot \epsilon$  for the isothermal case),  $I$  the identity tensor,  $\nabla u$  the displacement gradient (with the superscript  $T$  indicating the transpose) and  $\sigma$  the stress tensor (see Simha et al. [24] for details). In (2), the terms inside the parentheses in the integrand represent Eshelby's energy-momentum tensor [34]. As is customary in the asymptotic analysis of LEFM, the contour integral on  $\Gamma_{\text{front}}$  should be interpreted as a limit case when the distance to the singular crack tip tends to zero (i.e.,  $\Gamma_{\text{front}}$  tends to  $\Gamma_{\text{tip}}$ , see Fig. 2). Observe that the projection of the driving force vector in the direction of crack growth corresponds to the classical  $J$ -integral [35], which is commonly used to analyze growth of straight cracks.

Models using a sharp crack front require a constitutive relation between the driving force  $J_f$  (or the configurational force  $f_{\text{front}}$ ) and the crack front velocity  $v_f$ , which may include a nucleation criterion such as a critical value for propagation (e.g., critical energy release rate) and a criterion for the orientation of the vector  $v_f$  (e.g., the maximum dissipation criterion that stipulates that  $J_f$  and  $v_f$  are co-linear vectors that maximize their inner product).

### 2.2.2. Configurational force for a diffuse crack front

When the crack front is modeled using a cohesive zone approach, the configurational force needs to be reinterpreted. Effectively, the CZM is governed by the initiation and growth of the cohesive zone, which in turn is dependent upon a traction-separation relation that relates the cohesive traction to the crack opening. The effective configurational force is therefore associated to an integral around the cohesive zone as shown in Fig. 2.

The rate of energy dissipation  $D_f$  ascribed to the fracture process for cohesive zone modeling can be computed as

$$D_f = \int_{\Gamma_{\text{coh}}} \mathbf{t} \cdot \llbracket \mathbf{v}_c \rrbracket ds \quad (3)$$

where  $\mathbf{t} = \mathbf{t}^+ = -\mathbf{t}^-$  is the cohesive traction and  $\llbracket \mathbf{v}_c \rrbracket = \mathbf{v}^+ - \mathbf{v}^-$  is the crack opening rate with  $\mathbf{v}^\pm$  representing the material velocity on both sides of a partially-damaged crack front (see Fig. 2). Introducing the notion of an effective thermodynamical driving force  $\bar{J}_f$  and an effective crack front velocity  $\bar{v}_f$ , the effective rate of energy dissipation  $\bar{D}_f$  due to fracture can be expressed as

$$\bar{D}_f = \bar{J}_f \cdot \bar{v}_f, \quad (4)$$

with  $\bar{D}_f \geq 0$  for all admissible processes in accordance with the dissipation inequality. There are various possible ways to define the effective quantities, similar to the various scale transition approaches for multiscale fracture mechanics [36]. The relevant requirement is that the effective energy dissipated computed from (3) and the energy dissipation defined in (4) should coincide, i.e.,

$$\bar{D}_f = D_f. \quad (5)$$

For the purposes of the present work, the effective thermodynamical driving force is defined such that it coincides with the driving force for the sharp crack front case when the cohesive zone length tends to zero. To this end, let

$$\bar{J}_f = \int_{\Gamma_{\text{coh}}} (\phi \mathbf{I} - \nabla \mathbf{u}^T \boldsymbol{\sigma}) \mathbf{m} ds \quad (6)$$

hence, for the limit case of a infinitesimally small cohesive zone length, one has

$$\bar{J}_f \rightarrow -\mathbf{f}_{\text{front}} \quad \text{as} \quad \Gamma_{\text{coh}} \rightarrow \Gamma_{\text{tip}},$$

with the configurational force defined in (2).

In this approach, one can use (4) in combination with (3) and (5) to define the effective crack front velocity  $\bar{v}_f$  in the context of cohesive zone modeling. Since (4) involves an inner product (which only determines one scalar invariant of  $\bar{v}_f$ ), the complete determination of the vector requires use of an additional condition such as the maximum dissipation criterion that specifies the orientation of the vector. However, for the purposes of the present analysis, it is sufficient to *indirectly* determine the configurational force as indicated in the next section.

### 2.3. Relation between crack's configurational force, far field and inhomogeneities

From a modeling point of view, the constitutive relation for fracture within a sharp front approach is typically expressed as a relation between the crack front velocity and the thermodynamical driving force (or the configurational force). In contrast, the constitutive information for the cohesive zone modeling is typically expressed in the form of a relation between the cohesive traction and the crack opening. Correspondingly, the cohesive zone modeling does not explicitly define nor require a driving force or the magnitude of the crack front velocity in order to simulate the fracture process. It does require the orientation of the propagating crack, which is typically given in the same format as in the sharp crack front approach (e.g. in the form of a maximum dissipation criterion).

For both modeling approaches of the crack front (i.e., sharp crack front of LEFM or partially-damaged front of CZM), one can consider a neighborhood of the crack front  $\Omega$  as shown in Fig. 1. To facilitate the analysis of the effect of the cohesive zone length on the propagation of cracks in an heterogeneous medium, results are presented in terms of the configurational force in combination with the approach proposed in [24] for heterogeneous materials, which itself uses the notion of the  $J$ -integral method [35].

Noticing that Eshelby's energy-momentum tensor is discontinuous across the internal boundaries  $\Gamma_{\text{int}}$  and taking into account that the traction is zero on the fully-separated crack surfaces  $\Gamma_{\text{crack}}$ , the crack driving force is related to a far field integral and an internal boundary integral as follows:

$$\mathbf{J}_f = \mathbf{C}_{\text{far}} + \mathbf{C}_{\text{inh}} \quad (7)$$

where the far field term  $\mathbf{C}_{\text{far}}$  involves the integral along the boundary  $\Gamma_{\text{far}}$  of the energy-momentum tensor acting on the *outward* normal unit vector  $\mathbf{n}$ , i.e.,

$$\mathbf{C}_{\text{far}} = \int_{\Gamma_{\text{far}}} (\phi \mathbf{I} - \nabla \mathbf{u}^T \boldsymbol{\sigma}) \mathbf{n} ds \quad (8)$$

and the term  $\mathbf{C}_{\text{inh}}$ , which measures the contribution to the driving force due to the presence of inhomogeneities (in this case the particles), is given by the integral along the particle-matrix interface  $\Gamma_{\text{int}}$  of the jump of the energy-momentum tensor acting on the interface unit vector  $\mathbf{m}$ , i.e.,

$$\mathbf{C}_{\text{inh}} = - \int_{\Gamma_{\text{int}}} (\llbracket \phi \rrbracket \mathbf{I} - \langle \boldsymbol{\sigma} \rangle \llbracket \boldsymbol{\epsilon} \rrbracket) \mathbf{m} ds, \quad (9)$$

where it is noted that  $\mathbf{m}$  points away from the particle. The quantities  $\llbracket \bullet \rrbracket = \bullet^+ - \bullet^-$  and  $\langle \bullet \rangle = \frac{1}{2} (\bullet^+ + \bullet^-)$  represent, respectively, the jump and the average of the fields across the particle/matrix interface, with the superscript + and - representing the matrix and particle sides respectively.

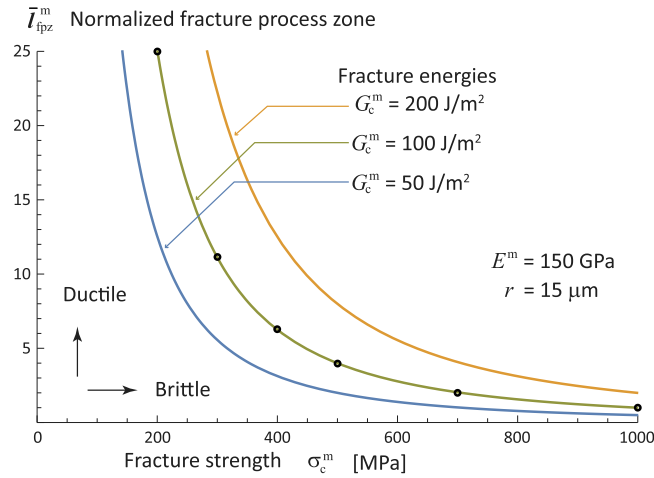


Fig. 3. Normalized process zone length  $\bar{l}_{fpz}^m$  as a function of the matrix mode I fracture strength  $\sigma_c^m$  for given values of the matrix Young's modulus  $E^m$  and a characteristic particle size  $r$  and for various values of the fracture energy  $G_c^m$ . The circles represent values used in the simulations.

Although the tractions and the displacements are continuous across the particle/matrix interface, the mismatch in the material properties induces discontinuities in the strain energy and the stress and strain tensors. Consequently, the term  $C_{inh}$  can be used to quantify the influence of the particles on the crack driving force. In turn, and of special interest for the present work, the stress and strain fields on the interface  $\Gamma_{int}$  are strongly influenced by the cohesive zone length scale if they are close enough to the crack front. This effect is quantified next through a series of representative numerical simulations.

### 3. Cohesive zone modeling and extended finite element method for crack problems

#### 3.1. Elastic and fracture material properties

The fracture process zone length (or cohesive zone length) is conventionally defined as

$$l_{fpz} := \frac{EG_c}{\sigma_c^2} \quad (10)$$

where  $E$  is a characteristic elastic stiffness of the material (typically Young's modulus),  $G_c$  and  $\sigma_c$  are, respectively, a characteristic fracture energy and fracture strength (typically mode I for a material that has an isotropic fracture response). For the present study, the properties of the cracked matrix material are used (denoted in the sequel with a superscript  $m$ ) and the crack length is normalized with respect to a characteristic dimension of the particles such as their radius  $r$  for circular inclusions (cylindrical in plane strain and spherical for the fully three-dimensional case). Consequently, the following non-dimensional parameter is subsequently used and also referred to as the cohesive zone length:

$$\bar{l}_{fpz}^m := \frac{l_{fpz}^m}{r} = \frac{E^m G_c^m}{r (\sigma_c^m)^2} \quad (11)$$

Plane strain deformation is assumed for all the simulations and isotropic linear elastic material properties are assumed for the bulk behavior of both the particle and the matrix. The Young's modulus of the matrix is taken as  $E^m = 150$  GPa and a stiffness mismatch ratio given by  $E^p/E^m = 3$  is considered, which is representative of particle-reinforced composites. The Poisson's ratio of the particle and the matrix are kept the same and equal to  $\nu = 0.25$ . The characteristic radius of the particles is taken as  $r = 15$   $\mu\text{m}$ . To study the effect of the particle in the presence of cohesive zone, the fracture process zone length is varied over a range by assigning various values for the cohesive strengths of both the particle and the matrix. The fracture energy is kept constant and equal to  $G_c^m = 100$  J/m<sup>2</sup>. Various values are given to the local cohesive strength value in the model, such as  $\sigma_c^m = 200, 300, 400, 500, 700, 1000$  MPa, which correspond to the process zone length scales,  $\bar{l}_{fpz}^m = 25, 11, 6.25, 4, 2$  and  $1$  respectively, obtained using (11) as shown in Fig. 3. A similar set of parameters can be achieved with a fixed fracture strength and a reduction in fracture energy, which in principle results in a more brittle-like fracture behavior. However, the parameter of interest here is the size of the fracture process zone in relation to the size of the particle, as defined by  $\bar{l}_{fpz}^m$ , with a more ductile behavior for large values and a more brittle behavior for low values.

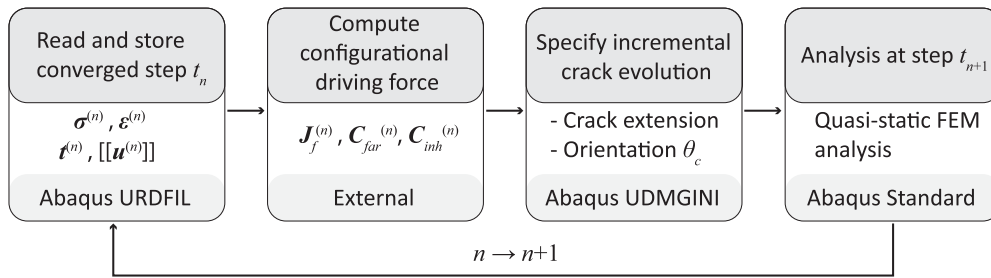


Fig. 4. Flow chart of incremental processing and postprocessing: The converged state at step  $n$ , corresponding to time  $t_n$ , is used to compute the configurational force, which then drives the crack evolution towards the next time step.

### 3.2. Numerical implementation

The numerical simulations using the cohesive zone model approach are carried in conjunction with the eXtended Finite Element Method (XFEM). This is a numerical technique to model discontinuities, such as cracks, and is an extension of the conventional continuous displacement-based finite element method. In XFEM, the presence of cracks is modeled by enriching the conventional bulk elements with additional displacement degrees of freedom to capture the crack openings [37–40]. Within the context of XFEM, the use of the level set method or similar techniques makes it possible to model arbitrary crack growth without remeshing [41]. As a result, the finite element mesh is not required to have the element boundaries aligned with the crack faces.

In the finite element software Abaqus, the XFEM implementation is available for modeling crack problems using two different fracture mechanics approaches [42]. One approach utilizes classical fracture mechanics solutions to enrich the crack tip and use virtual crack closure technique to simulate crack propagation. The second one relies on a surface-based cohesive zone model whereby a traction-separation relation governs the crack growth [39,43]. In this work, cohesive zone-based XFEM technique in Abaqus is utilized. The crack driving force and the crack direction are separately determined using configurational forces as described in the previous section. The implementation in Abaqus is indicated in Fig. 4. The stress, strain, cohesive traction and crack opening is extracted from the last converged step by means of the Abaqus Read Results File subroutine (URDFIL), which allows to post-process the data before the next time step. This is done in order to compute the next value of the configurational driving force using (7)–(9). Subsequently, this information is used in the Abaqus User-defined Damage Initiation subroutine (UDMGINI) to incrementally advance a crack. The UDMGINI subroutine allows to specify separately the crack extension and the crack orientation. Finally, a new time step is solved incrementally and the process is repeated (see [42] for more details).

The driving force is calculated to quantify the particle effect in the presence of process zone and further to provide crack propagation direction by using either the maximum energy dissipation criterion or the maximum principal stress criterion.

For the simulation of fracture, a quadratic stress criterion for crack initiation and a linear cohesive damage law is used for the damage evolution. The crack propagation direction is used as input for each increment during the analysis.

## 4. Effect of process zone length on crack driving force: Straight crack path

### 4.1. Simulation setup: A pair of symmetrically located particles

A two-dimensional  $L \times L$  square domain is considered for the analysis, which contains a symmetrically located pair of particles of diameter  $d = 2r$  each embedded in a matrix (see Fig. 5). The domain contains an initially straight edge crack of length  $a$  with its crack tip located at a horizontal distance  $b$  from the particles, which themselves are separated by a vertical distance  $c$  measured from the edge of the particles, as shown in Fig. 5. The horizontal distance is chosen as  $b = 7r$ , which is sufficiently large such that the influence of the particle on the crack driving force is initially negligible, regardless of the vertical distance  $c$  (see [3,4]). For the present simulations, the vertical distance is chosen as  $c = r$ . The domain size is chosen to be sufficiently large ( $L/r = 1000$ ) such that the boundary effects do not influence the results.

As indicated in Section 3.2, the normalized cohesive zone length values considered in the present analysis range from 25 (low strength) to 1 (high strength). Close to the particles, the characteristic mesh size is about  $1/20$  of the radius. Based on the most stringent case analyzed (smallest normalized cohesive length of 1, which is of the same size as the radius of the particle), the mesh used has about 20 elements to resolve the cohesive zone, which is enough for a relatively good convergence (compared to the rule of thumb of 3 to 5 elements).

Traction boundary conditions are specified on the top and the bottom edges of the domain. The configurational forces-based approach is employed in an explicit way to evaluate the crack driving force based on the deformation and stress fields of the previously converged time step. For the results shown in this section, the direction of crack extension is then determined based on the maximum dissipation criterion, which, due to symmetry, results in a straight horizontal crack path.

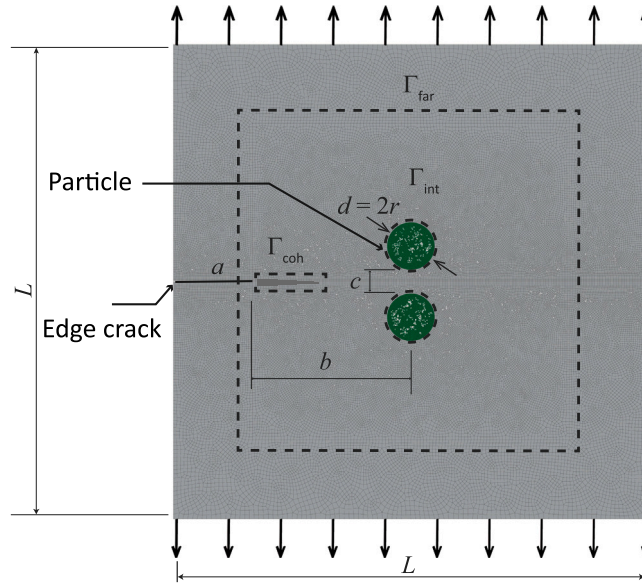


Fig. 5. Simulation model and mesh of the crack-particle system considered for the analysis. Two particles are placed symmetrically to the initial crack line, separated by a distance, given by  $c$ . The initial crack tip is located at a distance,  $b = 7r$ . The actual ratio  $L/r$  is 1000 (not shown to scale in the figure).

In accordance with the interpretation of the  $J$ -integral as work per unit cracked surface, consider the unit vector  $e$  in the direction of the crack propagation, i.e.,

$$e = \frac{\mathbf{v}_f}{|\mathbf{v}_f|}$$

where, as before,  $\mathbf{v}_f$  is the crack front velocity. For all simulations considered in this section, the corresponding crack paths are *straight*, which facilitates the comparison of the different results. To this end, it is convenient to present the results of the simulations in terms of the projections of the crack driving force and the inhomogeneous term in the direction of crack propagation, i.e.,

$$\bar{J}_f = \bar{J}_f \cdot e, \quad C_{inh} = C_{inh} \cdot e.$$

For the numerical integration around the crack front, the stress field is averaged within a neighborhood of three times the characteristic length (about  $1/20 \times 3 = 0.15$  times the radius). Since this value is also below (or at worst similar) to the recommended element size for resolving the cohesive zone length, then the results for the distinct cohesive zone lengths are not affected by the length scale parameter for averaging. Hence, the mesh is fine enough for resolving the cohesive zone length and the length scale for numerical averaging is also small enough such that the results for the distinct cohesive zone lengths are not affected by this parameter.

#### 4.2. Results and discussion

The results of the analysis for the case of two symmetrically placed particles are summarized in Fig. 6. The plot shows the relative contribution of the inhomogeneity integral term  $C_{inh}$  (associated with the presence of particles), normalized with respect to the (effective) fracture driving force  $\bar{J}_f$  for various locations of the crack front and for distinct values of the fracture process zone lengths (obtained by varying the cohesive strengths, as indicated in Fig. 3).

The positive values indicate that the presence of homogeneities require additional externally-provided energy for the crack growth compared to a homogeneous material (i.e., the so-called shielding effect of particles), whereas negative values indicate a tendency to facilitate crack growth since less externally applied energy is required for that process. As may be observed in Fig. 6, the changes in the configurational force associated with the particle strongly depend on the fracture process zone length. Correspondingly, in contrast to the classical fracture mechanics approach, the shielding effects of the particles directly depend on the process zone length. From the results it can be seen that the influence of the presence of the particle *increases*—in terms of the driving force contribution—with the *reduction* in the fracture process zone. The limit case of LEFM (infinitesimally small fracture process zone) corresponds to the maximum influence of the particles on the driving force.

To illustrate the above-mentioned effect, observe that for the length scale parameter given by  $\bar{l}_{fpz}^m = 25$ , the contribution of the particle to the crack driving force becomes relatively negligible as may be inferred from the figure. On the other hand, for  $\bar{l}_{fpz}^m = 1$ , the influence of the particle is the highest among the different cases considered. In particular, the positive peak occurs when the crack approaches the particle and is located at a distance equal to a radius of the particle from its center. The positive peak

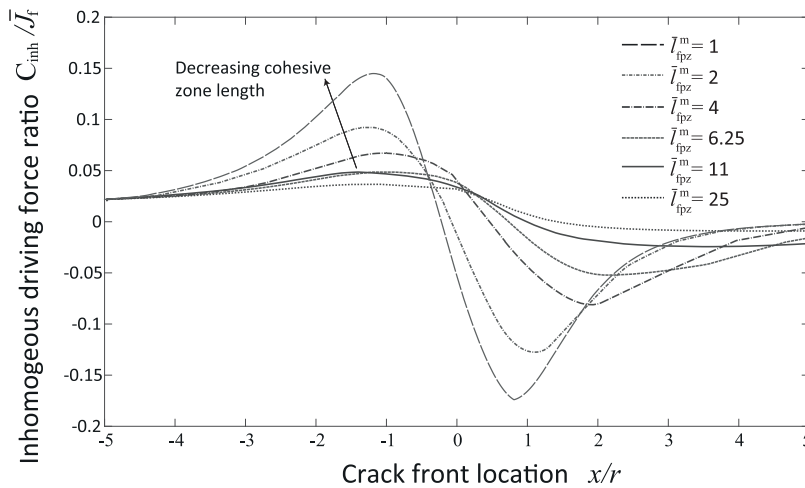


Fig. 6. Ratio of inhomogeneity term and crack driving force as a function of the crack front position for the case of symmetrically located particles with respect to the incoming crack and for various values of the fracture process zone length. The value  $x = 0$  corresponds to the midpoint between the particle centers.

corresponds to a normalized value of 0.15 reflecting the shielding effect of the particle because of its higher stiffness relative to the matrix. This would mean that for a crack to propagate a unit length (unit area in 3D), an additional energy of 15% (when compared to a homogeneous matrix case) is required to be dissipated in order to overcome the shielding effect of the particle when the crack is ahead of the particle. On the other hand, a negative peak would mean an anti-shielding effect attributed to the transition of the crack tip from stiffer to softer region. From the above results, it can be established that for a very large process zone length, the presence of a stiffness mismatched particle becomes relatively insignificant and does not have an observable influence on the crack kinetics.

From the previous analysis, it can be concluded that when the fracture process zone length is larger, the particles are effectively embedded in the diffused crack zone, which in turn reduces its influence on the change in the crack driving force.

To gain additional insight on this aspect, consider the spatial variation of the strength-normalized maximum in-plane stress,  $\bar{\sigma}_{\max}$ , which is defined as

$$\bar{\sigma}_{\max} := \frac{\sigma_{\max}}{\sigma_c} \quad (12)$$

where  $\sigma_{\max}$  is the maximum in-plane stress. The strength-normalized maximum in-plane stress is shown in Fig. 7 in the presence of a cohesive crack front ahead of the particles for varying fracture process zone lengths  $l_{fpz}$ .

From the stress field  $\bar{\sigma}_{\max}$  shown in the figure, it can be interpreted that the influence of the particle on the cohesive crack front is weaker as the process zone increases in size with respect to the particle size. Furthermore, the extension of the cohesive crack tip for a relatively large cohesive zone is governed majorly by the cohesive strength parameter, with the cohesive fracture energy playing only a secondary role for the cohesive crack extension.

In view of the previous results, it can be concluded that the shielding and antishielding influence of the inclusions in a matrix is significantly reduced for a relatively large fracture process zone. Equivalently, the effect of the particles is more pronounced in relatively brittle matrices. The effect needs to be considered during analyzing toughening mechanisms in heterogeneous materials, especially if the material's process zone length is large and more importantly if the inclusions in the material are smaller with respect to the process zone length.

## 5. Effect of process zone length: Curved/deflecting crack path

### 5.1. Simulation setup: A single asymmetrically located particle

In the previous section, the effect of the fracture process zone length on the particle shielding/ antishielding effects is quantified for a straight crack situation. In this section, the configurational forces are used to calculate the crack propagation direction and hence the crack paths in a cohesive zone fracture mechanics-XFEM framework. The objectives in this section are to (i) analyze the crack path as a function of fracture process zone length and (ii) compare the crack paths obtained using the maximum dissipation criterion and the maximum principal stress criterion, both within the context of cohesive XFEM.

The two-dimensional domain used for the analysis is similar to the case shown in Fig. 5, but with a *single* particle embedded in the matrix instead of two. The rest of the geometry is the same as the one shown in Fig. 5, including the initial crack and its offset with respect to the particle. The elastic and fracture properties of the matrix and the particle are kept the same as used in section 4.

$$\text{Strength-normalized maximum in-plane principal stress } \bar{\sigma}_{\max} = \frac{\sigma_{\max}}{\sigma_c^m}$$

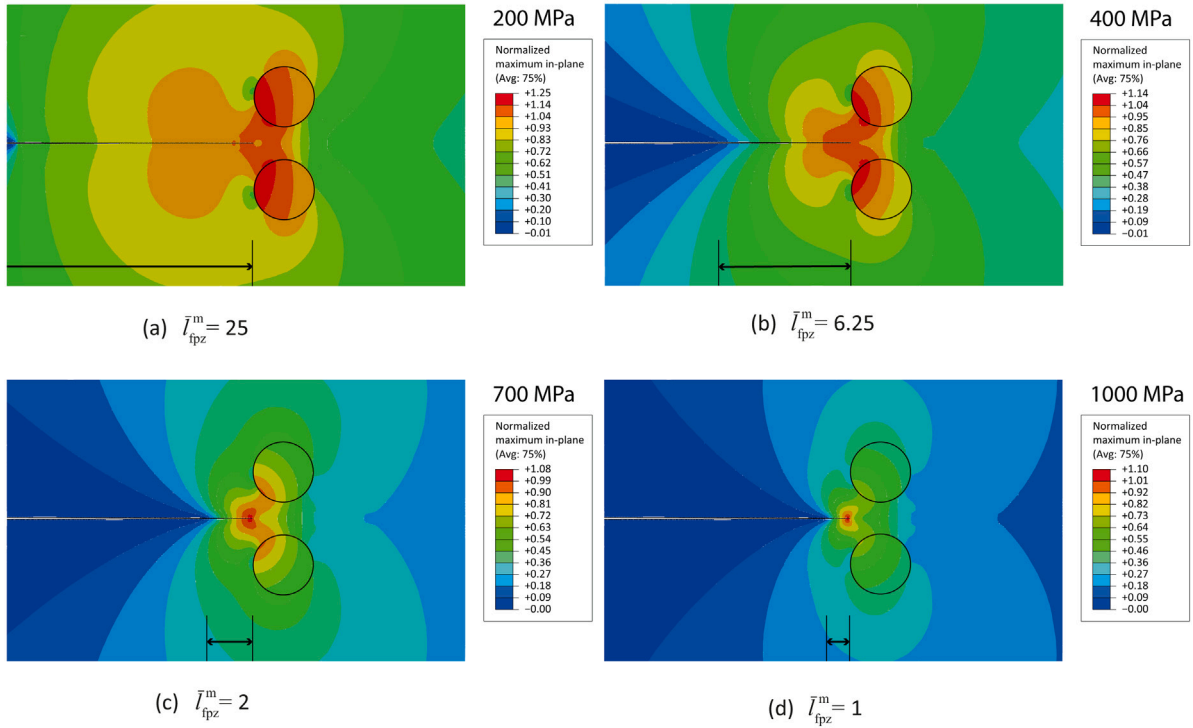


Fig. 7. Cohesive crack tip stress fields for varying fracture process zone lengths. The maximum in-plane principal stress is normalized with respect to the corresponding cohesive strength of the matrix material as indicated above the legend in each contour plot. The lines with two arrows indicate the approximate size of the active cohesive zone except for case (a) which extends beyond the region shown.

For the maximum energy dissipation criterion, the direction of crack propagation at each step can be obtained as follows:

$$\theta_c = \tan^{-1} \left( \frac{J_{f,2}}{J_{f,1}} \right) \quad (13)$$

In the above equation,  $J_{f,1}$  and  $J_{f,2}$  are the components of the crack driving force integral in a global coordinate system (in this case horizontal and vertical directions in the domain shown, respectively). The crack path angle  $\theta_c$  in (13), which coincides with the orientation of the crack front velocity vector  $\bar{v}_f$ , provides the maximum value for the dissipation  $\bar{D}_f$  given in (4) for a given magnitude of the crack front velocity.

For the maximum principal stress criterion, the orientation of the crack front velocity coincides with the direction of the maximum principal stress at the crack front. Within the theory of LEFM, for an elastic material that behaves isotropically from the point of view of fracture, the maximum dissipation criterion and the maximum principal stress criterion coincide. However, it is important to observe that in the context of a cohesive zone approach, these two criteria can provide distinct predictions due to the non-local nature of the theory, as shown below.

## 5.2. Results and discussion: Crack paths for distinct fracture process zone lengths

The results of the simulated crack paths and the associated crack driving forces are presented in Fig. 8 when using the maximum dissipation criterion. For conciseness, the results corresponding to selected length scale values are shown in the figures. Fig. 8 shows the relative contribution of the particle, measured by the term  $C_{inh}$ , to the crack driving force  $\bar{J}_f$ , with both quantities projected along the crack path. Although the path is not straight, it can be parametrized using its normalized  $x/r$ -coordinate.

From the Fig. 8, it can be inferred that, as the process zone length decreases, the influence of the particle increases, an observation similar to the symmetric particles case reported in section Section 4.2.

An interesting observation from the resulted crack paths is that, despite the stiffness mismatch ratio is kept the same for all reported simulations, the crack path is significantly different for distinct fracture process zone lengths, as shown in Fig. 9. In particular, if the process zone length is relatively large, the change in the crack trajectory is very small or even negligible. On the hand, if the fracture process zone length becomes small, the deflection in the crack path is more pronounced, as observed from

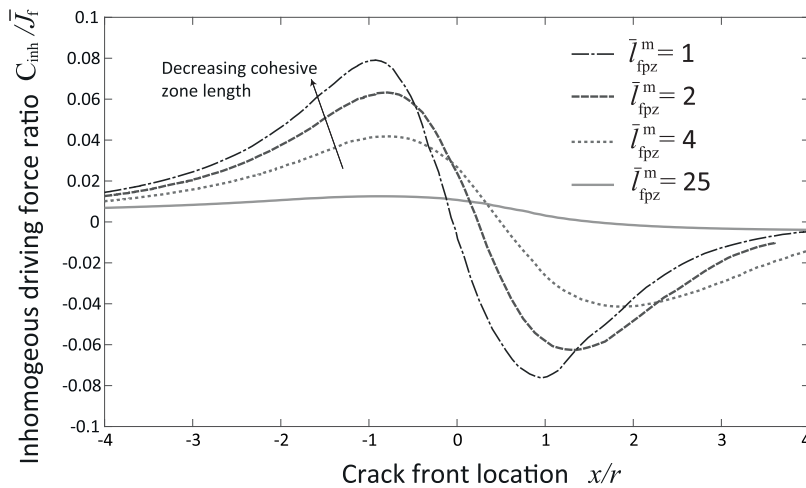


Fig. 8. Effect of fracture process zone length on crack driving force for a particle with an offset.

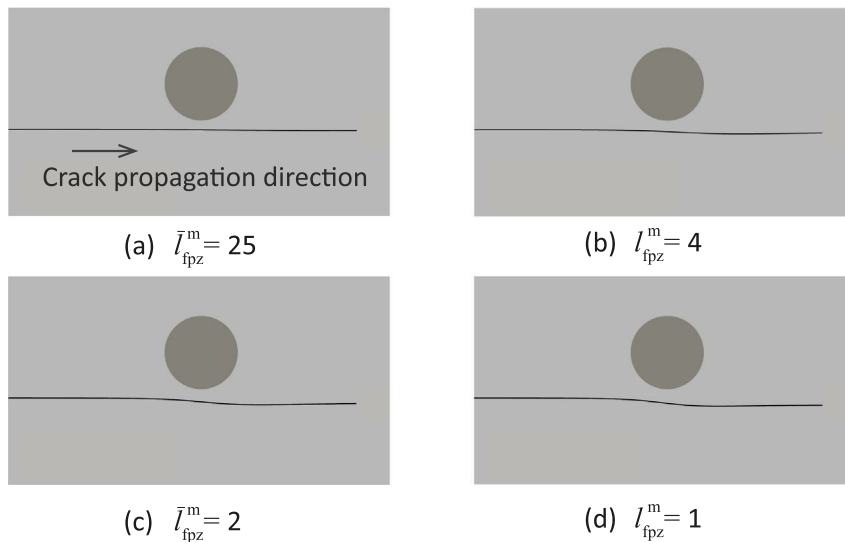


Fig. 9. Crack paths for distinct fracture process zone lengths. Same stiffness mismatch,  $E^p/E^m = 3$  of the particle with respect to the matrix is considered for all the four simulations.

the figure. For instance, the crack path corresponding to the case,  $\bar{l}_{fpz}^m = 25$  is almost straight, emphasizing a negligible influence of the particle on the resulting crack path. This is similar to the case observed in the previous section, whereby the change in crack driving force associated with the particle is close to zero if the fracture process zone length is very large as compared to the size of the particle. For the case of  $\bar{l}_{fpz}^m = 1$ , a relatively significant deflection of the crack path away from the particle is observed, see Fig. 9. In this case, the initially straight crack remains almost straight until it reaches a distance equal to one radius from the center of the particle, after which the deflection in the path is observed as determined by the maximum energy dissipation criterion.

For very low fracture process zone length scales, the crack path observed is similar to the one observed in the literature, where linear elastic fracture mechanics-based approach is used for crack path studies in combination with the maximum energy dissipation-based criterion for crack propagation direction prediction. This implies, that as the fracture process zone length becomes negligible, the results of the crack driving force and the crack path coincides with the linear elastic fracture mechanics results.

### 5.3. Comparison between two crack propagation criteria for crack direction

Although the maximum dissipation criterion is a widely used criterion in the formulation of fracture mechanics problems, the maximum principal stress criterion is also widely used, particularly in the context of XFEM [44–46]. Consequently, it is relevant to compare these two criteria in the context of distinct process zone lengths. For this study, the single particle-matrix system is solved

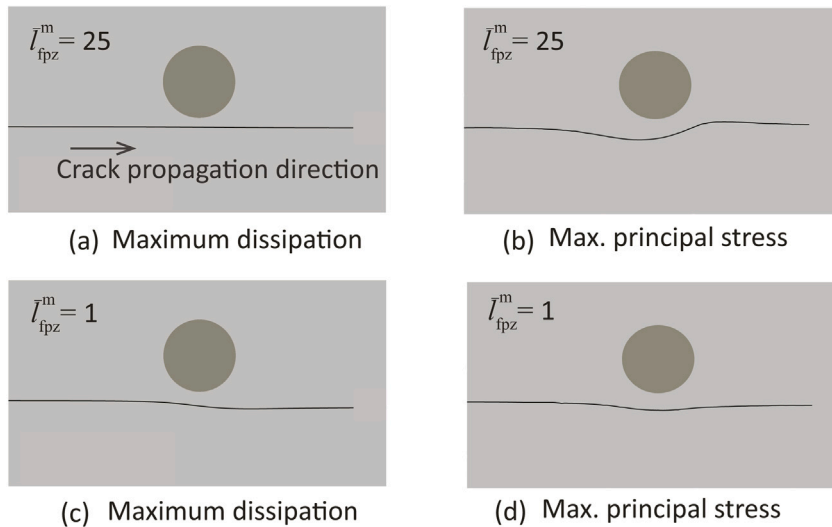


**Fig. 10.** Effect of crack propagation direction criterion on resulting crack path for two different process zone lengths. For all the four crack paths, stiffness mismatch ratio of the particle with respect to the matrix is the same and given by  $E^p/E^m = 3$ . Cases (a) and (c) correspond to cases (a) and (d) in Fig. 9 and are repeated here for convenience.

again but using the maximum principal stress criterion for two representative cases, namely  $\bar{l}_{fpz}^m = 25$  (large process zone) and  $\bar{l}_{fpz}^m = 1$  (small process zone).

The results for the comparative analysis are shown in Fig. 10 a and b for the larger fracture process zone length. From the results, it is clear that the two criteria predict different paths for the same material system. The maximum energy dissipation-based criterion predicts more or less a straight path. In contrast, the maximum principal stress-based criterion results in a noticeable crack deflection away from the particle. This implies that a stress-based direction criterion results in a deflected path even when the fracture process zone is very large, for which the influence of the particle is negligible if one observes the variation of the energy-based crack driving force contribution from the particle, see Fig. 6 and Fig. 8. Upon further comparison between the two criteria from Fig. 10 a and b, the initially straight crack starts to deflect away from the particle at a distance when the crack tip is approximately two radii away from the center of the particle. On the other hand, in the energy dissipation criteria, the crack starts to get deflected only when it reaches the edge of the particle, i.e., at a distance equal to one radius of the particle from its center. Further, once the crack deflects away from the particle and propagates further, an upward deflection is observed in the crack path resulting from principal stress-based criterion, whereas in the energy dissipation criterion, such an upward deflection is not observed.

The outcome of the simulations for the small fracture process zone length ( $\bar{l}_{fpz}^m = 1$ ) is shown in Fig. 10 c and d. In this case, both criteria predict a deflected crack path, albeit of a slightly different nature. Both crack paths approach and leave the particle with a relatively straight path (consistent with a global mode I crack), although the maximum dissipation criterion has a net downward shift, whereas the maximum principal stress criterion appears to continue at the same level as the incoming crack.

Upon comparing the crack paths for larger and smaller process zones using the maximum principal stress propagation criterion (cases (b) and (d) in Fig. 10), the deflection in the crack path close to the particle is less severe in the latter case. In general, it can be concluded that in particulate composites with a large number of inclusions, the maximum dissipation criterion and the maximum principal stress criterion will provide distinct predictions in the context of simulations using cohesive zone fracture mechanics. The differences can be traced back to the non-local nature of the crack driving force  $\bar{J}_f$  compared to the (local) stress tensor field in the vicinity of the crack front.

It is worth pointing out that both the maximum dissipation criterion and the maximum principal stress criterion are part of the constitutive model of a given material. As such, there is no intrinsic preference between one criterion or the other since a choice is made in terms of how accurately each criterion represents the fracture process in a given material. The main purpose of the comparative analysis is to highlight the differences between their predictions in the context of a particulate composite for distinct cohesive zone lengths, which can facilitate the choice of one criterion for modeling purposes.

## 6. Summary and conclusions

The effect of the process zone length in determining the contribution of the particles to crack driving force was analyzed using cohesive zone-based XFEM analysis together with the concept of configurational forces. This analysis highlights the differences between two entirely different fracture mechanics approaches, namely classical linear elastic fracture mechanics and cohesive zone fracture mechanics. Finally, a comparison between different crack propagation direction criteria was discussed with varying fracture process zone lengths. The following conclusions and insights were drawn from the analyses:

- The process zone length significantly influences the contribution of the particle to the crack driving force. In particular, a cohesive crack with larger fracture process zone length does not feel the presence of the particle ahead of the cohesive crack tip. On the other hand, in case of a smaller process zone, the influence of the particle on the crack driving force is much more pronounced.
- The crack path is also significantly affected by the fracture process zone length. Lesser the process zone length with respect to the particle size, larger is the deflection in the crack trajectory. For the same stiffness mismatch ratio, different crack trajectories are observed depending on the length of the fracture process zone. For a stiffness mismatch of 3 (stiffer particle), the crack path is almost straight if the process zone is large, an observation distinctly different from classical fracture mechanics based approaches. This suggests that the process zone is an important parameter in determining the effective toughness of a particulate composite, especially that involves cohesive ductile-like fracture instead of brittle fracture.
- The choice of criterion for the direction of crack propagation may significantly influence the predicted crack path. Using the maximum energy dissipation criterion for crack direction, no or little crack deflection is observed for larger process zone lengths, whereas deflection is observed for smaller process zone lengths. On the other hand, the criterion for crack propagation based on the maximum principal stress predicts a deflected path irrespective of the length of the fracture process zone. A stronger deflection is observed for larger process zone case. For smaller process zone length, both criteria tend to predict somewhat similar crack paths in relation to the larger process zone case. The final choice of a criterion typically will depend on which one represents the actual fracture process more accurately for a given composite material.

### CRedit authorship contribution statement

**Sathiskumar Anusuya Ponnusami:** Writing – original draft, Methodology, Software, Validation, Investigation, Conceptualization, Formal analysis. **Jayaprakash Krishnasamy:** Writing – original draft, Validation, Software, Investigation, Formal analysis. **Sergio Turteltaub:** Writing – review & editing, Conceptualization, Formal analysis, Funding acquisition, Methodology, Project administration, Supervision, Validation. **Sybrand van der Zwaag:** Writing – review & editing, Validation, Supervision, Project administration, Investigation, Funding acquisition, Formal analysis.

### Declaration of competing interest

The authors declare that they have no known competing financial interests or personal relationships that could have appeared to influence the work reported in this paper.

### Acknowledgment

This work was funded in part by the European Union's seventh framework program (FP7) through the NMP SAMBA project (grant number 309849).

### References

- [1] Lipetzky P, Knesl Z. Crack-particle interaction in a two-phase composite part II: crack deflection. *Int J Fract* 1985;73(1):81–92.
- [2] Li R, Chudnovsky A. Energy analysis of crack interaction with an elastic inclusion. *Int J Fract* 1993;63(3):247–61.
- [3] Bush M. The interaction between a crack and a particle cluster. *Int J Fract* 1997;88(3):215–32.
- [4] Knight M, Wrobel L, Henshall J, De Lacerda L. A study of the interaction between a propagating crack and an uncoated/coated elastic inclusion using the BE technique. *Int J Fract* 2002;114(1):47–61.
- [5] Kitey R, Phan A-V, Tippur H, Kaplan T. Modeling of crack growth through particulate clusters in brittle matrix by symmetric-Galerkin boundary element method. *Int J Fract* 2006;141(1–2):11–25.
- [6] Ayyar A, Chawla N. Microstructure-based modeling of crack growth in particle reinforced composites. *Compos Sci Technol* 2006;66(13):1980–94.
- [7] Williams R, Phan A-V, Tippur H, Kaplan T, Gray L. SGBEM analysis of crack particle(s) interactions due to elastic constants mismatch. *Eng Fract Mech* 2007;74(3):314–31.
- [8] Lipetzky P, Schmauder S. Crack-particle interaction in two-phase composites part I: Particle shape effects. *Int J Fract* 1994;65(4):345–58.
- [9] Nandy M-O, Schmauder S, Kim B-N, Watanabe M, Kishi T. Simulation of crack propagation in alumina particle-dispersed SiC composites. *J Eur Ceram Soc* 1999;19(3):329–34.
- [10] Ayyar A, Chawla N. Microstructure-based modeling of the influence of particle spatial distribution and fracture on crack growth in particle-reinforced composites. *Acta Mater* 2007;55(18):6064–73.
- [11] Natarajan S, Kerfriden P, Mahapatra DR, Bordas S. Numerical analysis of the inclusion-crack interaction by the extended finite element method. *Int J Comput Methods Eng Sci Mech* 2014;15(1):26–32.
- [12] Anderson TL. *Fracture mechanics: fundamentals and applications*. CRC Press; 2005.
- [13] Kim Y, Allen D, Seidel G. Damage-induced modeling of elastic-viscoelastic randomly oriented particulate composites. *J Eng Mater Technol* 2006;128(1):18–27. <http://dx.doi.org/10.1115/1.2127960>.
- [14] Meng Q, Wang Z. Prediction of interfacial strength and failure mechanisms in particle-reinforced metal-matrix composites based on a micromechanical model. *Eng Fract Mech* 2015;142:170–83. <http://dx.doi.org/10.1016/j.engfracmech.2015.06.001>.
- [15] Dastgerdi JN, Anbarlooie B, Marzban S, Marquis G. Mechanical and real microstructure behavior analysis of particulate-reinforced nanocomposite considering debonding damage based on cohesive finite element method. *Compos Struct* 2015;122:518–25. <http://dx.doi.org/10.1016/j.compstruct.2014.12.009>.
- [16] Gentieu T, Catapano A, Jumel J, Broughton J. A mean-field homogenisation scheme with CZM-based interfaces describing progressive inclusions debonding. *Compos Struct* 2019;229. <http://dx.doi.org/10.1016/j.compstruct.2019.111398>.
- [17] Wang JT. Relating cohesive zone model to linear elastic fracture mechanics. *NASA technical report*, 2010.

- [18] Jin Z-H, Sun C. A comparison of cohesive zone modeling and classical fracture mechanics based on near tip stress field. *Int J Solids Struct* 2006;43(5):1047–60.
- [19] Rabinovitch O. Debonding analysis of fiber-reinforced-polymer strengthened beams: Cohesive zone modeling versus a linear elastic fracture mechanics approach. *Eng Fract Mech* 2008;75(10):2842–59.
- [20] Abedi R. A comparative and parametric study of dynamic cohesive and linear elastic fracture mechanics models. *Int J Solids Struct* 2016;102:163–75.
- [21] Chen C-R, Mai Y-W. Comparison of cohesive zone model and linear elastic fracture mechanics for a mode I crack near a compliant/stiff interface. *Eng Fract Mech* 2010;77(17):3408–17.
- [22] Parmigiani J, Thouless M. The roles of toughness and cohesive strength on crack deflection at interfaces. *J Mech Phys Solids* 2006;54(2):266–87.
- [23] Gurtin ME. *Configurational forces as basic concepts of continuum physics*. Vol. 137. Springer Science & Business Media; 2008.
- [24] Simha N, Fischer F, Kolednik O, Predan J, Shan G. Crack tip shielding or anti-shielding due to smooth and discontinuous material inhomogeneities. *Int J Fract* 2005;135(1–4):73–93.
- [25] Gurtin ME, Podio-Guidugli P. Configurational forces and a constitutive theory for crack propagation that allows for kinking and curving. *J Mech Phys Solids* 1998;46(8):1343–78.
- [26] Gurtin ME, Podio-Guidugli P. Configurational forces and the basic laws for crack propagation. *J Mech Phys Solids* 1996;44(6):905–27.
- [27] Nguyen T, Govindjee S, Klein P, Gao H. A material force method for inelastic fracture mechanics. *J Mech Phys Solids* 2005;53(1):91–121.
- [28] Simha N, Fischer F, Shan G, Chen C, Kolednik O. J-integral and crack driving force in elastic–plastic materials. *J Mech Phys Solids* 2008;56(9):2876–95.
- [29] Özenç K, Kaliske M, Lin G, Bhashyam G. Evaluation of energy contributions in elasto-plastic fracture: a review of the configurational force approach. *Eng Fract Mech* 2014;115:137–53.
- [30] Kolednik O, Predan J, Fischer F. Reprint of cracks in inhomogeneous materials: Comprehensive assessment using the configurational forces concept. *Eng Fract Mech* 2010;77(18):3611–24.
- [31] Kolling S, Baaser H, Gross D. Material forces due to crack-inclusion interaction. *Int J Fract* 2002;118(3):229–38.
- [32] Kolednik O, Predan J, Shan G, Simha N, Fischer FD. On the fracture behavior of inhomogeneous materials—a case study for elastically inhomogeneous bimaterials. *Int J Solids Struct* 2005;42(2):605–20.
- [33] Chen C, Pascual J, Fischer F, Kolednik O, Danzer R. Prediction of the fracture toughness of a ceramic multilayer composite—modeling and experiments. *Acta Mater* 2007;55(2):409–21.
- [34] Eshelby J. The elastic energy-momentum tensor. *J Elasticity* 1975;5(3–4):321–35.
- [35] Rice J. A path independent integral and approximate analysis of strain concentration by notches and cracks. *J Appl Mech* 1968;35(2):379+. <http://dx.doi.org/10.1115/1.3601206>.
- [36] Turteltaub S, Suarez-Millan R. Energetically-consistent multiscale analysis of fracture in composites materials. *Eur J Mech A Solids* 2020;84. <http://dx.doi.org/10.1016/j.euromechsol.2020.104079>.
- [37] Belytschko T, Black T. Elastic crack growth in finite elements with minimal remeshing. *Internat J Numer Methods Engrg* 1999;45(5):601–20.
- [38] Dolbow J, Belytschko T, et al. A finite element method for crack growth without remeshing. *Internat J Numer Methods Engrg* 1999;46(1):131–50.
- [39] Moës N, Belytschko T. Extended finite element method for cohesive crack growth. *Eng Fract Mech* 2002;69(7):813–33.
- [40] Fries T-P, Belytschko T. The extended/generalized finite element method: an overview of the method and its applications. *Internat J Numer Methods Engrg* 2010;84(3):253–304.
- [41] Stolarska M, Chopp D, Moës N, Belytschko T. Modelling crack growth by level sets in the extended finite element method. *Internat J Numer Methods Engrg* 2001;51(8):943–60.
- [42] ABAQUS. Version 6.14 documentation. Providence, RI, USA: Dassault Systemes Simulia Corp. 2011.
- [43] Remmers JJ, de Borst R, Needleman A. The simulation of dynamic crack propagation using the cohesive segments method. *J Mech Phys Solids* 2008;56(1):70–92.
- [44] Mergheim J, Kuhl E, Steinmann P. A finite element method for the computational modelling of cohesive cracks. *Internat J Numer Methods Engrg* 2005;63(2):276–89.
- [45] Wells GN, Sluys L. A new method for modelling cohesive cracks using finite elements. *Internat J Numer Methods Engrg* 2001;50(12):2667–82.
- [46] Mariani S, Perego U. Extended finite element method for quasi-brittle fracture. *Internat J Numer Methods Engrg* 2003;58(1):103–26.